

ORIGINAL ARTICLE

Daytime spikes in dopaminergic activity drive rapid mood-cycling in mice

MM Sidor^{1,2}, SM Spencer², K Dzirasa³, PK Parekh¹, KM Tye⁴, MR Warden⁵, RN Arey², JF Enwright III^{2,6}, JPR Jacobsen⁷, S Kumar³, EM Remillard⁶, MG Caron³, K Deisseroth⁸ and CA McClung^{1,2}

Disruptions in circadian rhythms and dopaminergic activity are involved in the pathophysiology of bipolar disorder, though their interaction remains unclear. Moreover, a lack of animal models that display spontaneous cycling between mood states has hindered our mechanistic understanding of mood switching. Here, we find that mice with a mutation in the circadian *Clock* gene (*Clock* Δ 19) exhibit rapid mood-cycling, with a profound manic-like phenotype emerging during the day following a period of euthymia at night. Mood-cycling coincides with abnormal daytime spikes in ventral tegmental area (VTA) dopaminergic activity, tyrosine hydroxylase (TH) levels and dopamine synthesis. To determine the significance of daytime increases in VTA dopamine activity to manic behaviors, we developed a novel optogenetic stimulation paradigm that produces a sustained increase in dopamine neuronal activity and find that this induces a manic-like behavioral state. Time-dependent dampening of TH activity during the day reverses manic-related behaviors in *Clock* Δ 19 mice. Finally, we show that CLOCK acts as a negative regulator of TH transcription, revealing a novel molecular mechanism underlying cyclic changes in mood-related behavior. Taken together, these studies have identified a mechanistic connection between circadian gene disruption and the precipitation of manic episodes in bipolar disorder.

Molecular Psychiatry advance online publication, 6 January 2015; doi:10.1038/mp.2014.167

INTRODUCTION

Bipolar disorder is a complex psychiatric illness that presents with abnormal mood states ranging from anxiety and depression to altered activity levels and disrupted sleep-wake cycles. Mood-cycling, or switching, between manic, depressive and euthymic mood states is a hallmark feature of bipolar disorder, yet insight into its mechanistic driving force has remained highly elusive. Compelling evidence suggests that altered circadian clocks are involved in the psychopathology of bipolar disorder,¹ as disrupted circadian rhythms often predict the onset of mood episodes and can, themselves, precipitate depression or mania in susceptible individuals.^{2,3} Previously, we demonstrated that mice with a point mutation in the *Clock* gene (*Clock* Δ 19),^{4,5} a core regulatory component of the circadian transcriptional machinery, display a behavioral profile during the daytime (that is, their inactive period) that is strikingly similar to the manic phase of human bipolar disorder, and includes hyperactivity, increased reward-related behaviors and decreased anxiety- and depressive-like behaviors.^{3,6} This behavioral profile is concurrent with increased firing of ventral tegmental area (VTA) dopamine cells.^{6,7} Indeed, converging lines of evidence point to altered mesolimbic dopaminergic activity as a prominent mediator of human mania. For instance, psychostimulant exposure produces a behavioral state similar to bipolar mania and the dopamine precursor, L-dopa can precipitate mania in patients.⁸ In turn, administration of alpha-methyl-para tyrosine (AMPT), an inhibitor of the rate-limiting enzyme in

dopamine synthesis, tyrosine hydroxylase (TH), can decrease manic symptoms.⁸ Interestingly, direct knockdown of *Clock* in the VTA of wild-type mice recapitulates the reduced anxiety-related phenotypes typical of manic-like behavior in *Clock* Δ 19 mice, but also leads to increased depression-related behavior,⁹ hinting at a potential role for *Clock* in regulating VTA dopaminergic activity and distinct mood states. However, it is currently unclear how manic episodes are precipitated and what molecular mechanisms underlie this process. Given this, we first sought to establish a direct and functionally significant link between the diurnal activity of VTA dopaminergic activity and mood-related behavior. Optogenetics was used to enable direct control of VTA dopamine neuronal firing to determine to what extent VTA dopamine activity drives select features of manic-like behavior. Whereas most studies using optogenetics have examined the effects of acute neural circuit modulation, here, we introduce a novel optogenetic paradigm to induce chronic changes in VTA neural activity. In addition, we sought to determine the molecular mechanisms by which the circadian *Clock* gene regulates dopaminergic activity.

MATERIALS AND METHODS

Animals

Clock Δ 19 mutant mice were created by *N*-ethyl-*N*-nitrosourea mutagenesis that produces a dominant-negative CLOCK protein defective in transcriptional activity.⁵ For all experiments using *Clock* Δ 19 mutants, adult male

¹Department of Psychiatry, University of Pittsburgh Medical School, Pittsburgh, PA, USA; ²Department of Psychiatry, UT Southwestern Medical Center, Dallas, TX, USA; ³Department of Psychiatry and Behavioral Sciences, Center for Neuroengineering, Duke University Medical Center, Durham, NC, USA; ⁴Department of Brain and Cognitive Sciences, Picower Institute for Learning and Memory, Massachusetts Institute of Technology, Cambridge, MA, USA; ⁵Department of Neurobiology and Behavior, Cornell University, Ithaca, NY, USA; ⁶Department of Biology, Austin College, Sherman, TX, USA; ⁷Department of Cell Biology, Duke University Medical Center, Durham, NC, USA and ⁸Departments of Bioengineering and Psychiatry and Behavioral Sciences, Stanford University, Stanford, CA, USA. Correspondence: Dr CA McClung, Psychiatry, University of Pittsburgh Medical School, 450 Technology Drive, Suite 223, Pittsburgh, 15219, PA, USA.

E-mail: McClungca@upmc.edu

Received 14 July 2014; revised 3 October 2014; accepted 20 October 2014

mutant (Clock/Clock) and wild-type (+/+) littermate controls, on a mixed BALB/c, C57BL/6 background, were group housed in sets of two to four per cage. Optogenetic studies were carried out on adult male TH::IRES-Cre transgenic mice (EM:00254).¹⁰ TH::Cre mice were individually housed following surgery to reduce damage to the permanent fiber optic implants. All mice were maintained on a 12/12-h light/dark cycle (lights on 7:00 a.m. = Zeitgeber (ZT) 0, lights off at 7:00 p.m. = ZT 12) with food and water provided *ad libitum*. Cohorts of animals that underwent behavioral testing at night were maintained on a reverse light/dark cycle (lights on at 7:00 p.m.). Adult male C57BL/6 mice (Jackson Laboratories, Bar Harbor, ME, USA) were used for chromatin immunoprecipitation (ChIP) assays. All animal use was conducted in accordance with the National Institute of Health guidelines and approved by the Institutional Animal Care and Use Committees of the University of Pittsburgh, UT Southwestern Medical Center, Duke University, and Stanford University.

Electrophysiology

Surgeries. Male *Clock* Δ 19 and WT littermate controls (20–30-weeks old) were used for electrophysiological experiments. Mice were anesthetized with ketamine (100 mg kg⁻¹) and xylazine (10 mg kg⁻¹), placed in a stereotaxic device, and metal ground screws were secured to the cranium. A total of 14 tungsten microwires were arranged in bundle arrays of 4–10 wires (each wire separated by at least 250 μ m), and implanted to target the dorsal hippocampus and VTA. Implanted coordinates were as follows (all coordinates are measured from bregma): dorsal hippocampus, AP – 2.3 mm, ML +1.63 mm, DV – 1.3 mm; VTA, AP – 3.2 mm, ML +0.3 mm, DV – 4.25 mm. Implanted electrodes were anchored to ground screws using dental acrylic. After a 2-week recovery period, mice were then separated into individual cages and their cage placed into the recording chamber. Following a 2-day habituation period, neurophysiological data were recorded throughout the entire 24-h light/dark cycle of each mouse.

Neuronal and local field potential data acquisition. Neuronal activity was sorted online and recorded using the Multi-Neuron Acquisition Processor system (Plexon, Dallas, TX, USA). Local field potentials were pre-amplified (500 \times), filtered (0.7–170 Hz) and digitized at 500 Hz using a Digital Acquisition card (National Instruments, Austin, TX, USA) and a Multi-Neuron Acquisition Processor (Plexon). Bursting and firing rate analyses were performed using Neuroexplorer (Nex Technologies, Littleton, MA, USA). Electrophysiological recordings were referenced to two ground screws located above the cerebellum and anterior cortex. VTA channels were thresholded to select for dopaminergic neurons based on standard physiological criteria including waveforms >2 ms in length and bursting.^{6,11,12} Cells were sorted using an offline-sorting algorithm (Plexon) to confirm the quality of recorded cells. For firing analysis, data were collected during 60-s epochs of rapid eye movement (REM) sleep occurring during each of the 6-h intervals: ZT0–6, ZT6–12, ZT12–18 and ZT18–24. As several mutant mice failed to display a 60 s epoch of REM sleep during each of the four time windows, additional inclusion criteria were applied such that neurons had to display a minimum firing rate of 1.5 Hz and at least one bursting episode during the 60-s period. Burst events were initiated by a pair of spikes having an interspike interval of 80 ms and terminated by interspike intervals of 160 ms. Following initial analysis, we also performed within neuronal analysis where only neurons recorded during the first 6 h of the light and dark cycle were included.

Behavioral state identification. Behavioral states were identified using a two-dimensional state map as previously described.¹³ The state map generated cluster separation based on the high amplitude theta (4–9 Hz) and gamma (33–55 Hz) oscillations characteristic of REM sleep, the absence of gamma oscillations and high amplitude delta (1–4 Hz) characteristic of slow-wave sleep, and the high amplitude gamma and theta oscillations characteristic of waking. Behavioral state maps were generated from each of the two to four hippocampal local field potentials acquired; the map that produced the best cluster separation was utilized for behavioral state identification.

Optrode construction and implantation

Two- to 3-month-old TH::Cre mice were anesthetized with isoflurane and placed in a stereotaxic device. Metal ground screws were secured to the skull above the cerebellum and anterior cranium. A total of eight tungsten microwires were arranged in a bundle (each wire separated by at least 200 μ m), and implanted in the VTA as follows (AP – 3.4 mm, ML +0.3 mm

and DV – 4.25 mm, relative to bregma). Full details of the procedures for electrode construction and surgical implantation have been previously described.¹⁴ A mono fiberoptic cannula coupled to a 2.5 mm metal ferrule (NA 0.22; 100 μ m (inner diameter), 125 μ m buffer (outer diameter), MFC 100/125-0.22, Doric Lenses, Quebec, QC, Canada) was built directly into the microarray bundle prior to surgical implantation. The tip of the fiber was secured 500 μ m above the tip of the tungsten microwires such that the optical fiber lay just above the VTA following implantation. Implanted electrodes were anchored to ground screws using dental acrylic. Optogenetic stimulation experiments were initiated following a 25-day recovery period.

Optogenetics

Virus construction and packaging. Recombinant adeno-associated virus type 5 (AAV₅)-DIO-Ef1a-hChR2 (C128S/D156A)-enhanced yellow fluorescence protein (eYFP) vector and its control vector, AAV₅-DIO-Ef1a-eYFP, were constructed by cloning DIO-Ef1a-hChR2 (C128S/D156A)-eYFP and DIO-Ef1a-eYFP, respectively, into an AAV backbone using MluI and EcoRI restriction sites. The resulting plasmid DNA was serotyped with AAV₅ coat proteins and packaged by the University of North Carolina viral vector core.

Light transmission calculations for optical fiber placement. Fiber optic placement was calculated to ensure light propagation throughout the entire extent of the VTA while maintaining adequate light power to achieve optimal opsin activation based on known stable step-function opsin (SSFO) photocurrent responses.¹⁵ Fiber placement was determined by taking into account both the medial-lateral (ML) spread of light and the dorsal-ventral (DV) transmission of light. ML spread was calculated using trigonometry based on light emission from a single point source, where the half angle of divergence (θ_{div}) is given by:

$$\theta_{div} = \sin^{-1} \left(\frac{NA_{fiber}}{n_{tissue}} \right)$$

where NA is the numerical aperture of the fiber (0.22) and n_{tissue} is the refractive index of light as it travels through gray matter (1.36).¹⁶ To calculate distance, the fractional change in light power (mW) that occurs as light travels through a medium was taken into consideration. This is based on both the fractional loss of light that occurs with conical spread and light scattering.^{17,18} The corresponding power densities (mW mm⁻²) were then calculated for varying distances of fiber tip from viral placement through the entire DV extent of the VTA using the online calculator for light transmission (<http://www.stanford.edu/group/dlab/cgi-bin/graph/chart.php>). ML spread (radius of illumination) was then calculated using the most ventral distance within the VTA that achieved power densities required to activate SSFO.

Stereotaxic viral injection and optical fiber implantation. TH::Cre mice were anaesthetized with 1.5–3.0% isoflurane and kept on a self-regulating heating pad throughout the duration of the stereotaxic surgery. Purified AAV₅ virus (viral titer = 4×10^{12} viral molecules per ml) was unilaterally injected into the VTA at AP – 3.3, ML +0.44, DV – 4.2 and – 4.7 (relative to bregma) using a 5-mm long 33-gauge metal beveled needle, facing medial. A 10 μ l Hamilton microsyringe (nanofil; WPI, Sarasota, FL, USA) and its controller (Micro4; WPI) delivered 1 μ l of virus at each DV coordinate at a rate of 0.1 μ l min⁻¹. The needle was left in place for 10 min between injections and slowly withdrawn. Immediately following, a Doric chronically implantable optical fiber (NA = 0.22, 200 μ m inner core, Doric Lenses) was cut to a length of ~5 mm and unilaterally implanted over the VTA at – 4.1 mm DV. Light transmission through each fiber was measured before implantation and confirmed post-mortem. Only fibers with \geq 80% transmission efficiency were used. Adhesive cement (C&B metabond, Parkell, Edgewood, NY, USA) and cranioplastic cement (Dental cement, Stoelting, Wood Dale, IL, USA) were used to secure the fiber optic implant to the skull and the incision was closed and sealed with tissue adhesive (Vetbond; Fisher, Pittsburgh, PA, USA). All surgeries were performed using strict aseptic techniques. Mice were administered 0.5 ml of 0.9% saline and Buprenex (0.1 mg kg⁻¹) sub-cutaneously immediately following surgery. After recovery, mice were left undisturbed for 4 weeks to allow for sufficient viral expression prior to behavioral testing.

In vivo light delivery. For chronic stimulation, TH::Cre mice were individually placed into KinderScientific locomotor boxes (Poway, CA, USA; see Behavioral Assays for more details) and simultaneously received a single unilateral 5 s pulse of blue light every 15 min for 1 h between ZT6–10

(daytime) or ZT18–22 (nighttime) for 7 consecutive days. A multi-mode fiber optic black-jacketed patchcord (NA 0.22, 200 μm inner core, Doric Lenses) connected a 100 mW 473 nm diode-pumped solid-state laser or a 100 mW 447 nm diode laser (OEM Lasers Systems, East Lansing, MI, USA) to permanently implanted fiber optics. Commutators (Doric Lenses) were used to reduce torque on patchcords that occurs with animal movement. A standard power meter (Thorlabs, Newton, NJ, USA) was used to measure the emitted light power prior to fiber tethering to achieve a minimum of 3 mW at fiber tip (corresponding power densities of 39–3 mW mm^{-2} at VTA depths of 0.1–0.6 m). Laser output was controlled using a Rigol pulse generator (DG1022, Rigol USA, Oakwood Village, OH, USA).

Immunohistochemistry. Mice were perfused with 4% paraformaldehyde in 1 \times phosphate-buffered saline (PBS) (pH 7.4) and the brains transferred to a 30% sucrose solution. Forty micrometer sections were taken and processed for TH and DAPI. Briefly, floating sections were rinsed in 1 \times PBS to remove the cryoprotectant/fixative. Sections were then blocked in PBS+ + (3% Normal Donkey Serum, 0.3% Triton-X in PBS) for 30 min and incubated with a chicken anti-TH primary antibody (1:500, Aves Labs, Tigard, OR, USA) overnight at 4 $^{\circ}\text{C}$ on a rotary shaker. The following day, sections were rinsed in 1 \times PBS and incubated in a donkey anti-chicken secondary conjugated to Cy5 (1:500, Jackson ImmunoResearch Laboratories, West Grove, PA, USA) for 3 h at room temperature (RT) on a rotary shaker. Sections were then incubated with DAPI (1:50 000) for 20 min, washed and mounted on microscope slides with PVA-DABCO. For cFOS/GFP double labeling shown in Supplementary Figure 3, 30 μm were blocked for 1 h and incubated with mouse anti-TH primary antibody (1:5000, Sigma, St. Louis, MO, USA) and adjacent sections incubated with rabbit anti-GFP (1:20 000, Abcam, Cambridge, MA, USA) and goat anti-cFOS (1:250, Santa Cruz Biotechnology, Dallas, TX, USA) overnight at RT. The following day, sections were rinsed in 1 \times PBS and incubated in the species-appropriate secondary conjugated to various fluorophores (1:400, Invitrogen, Grand Island, NY, USA) for 2 h at RT on a rotary shaker. Sections were then washed in 1 \times PBS, mounted and coverslipped with DAPI mounting medium (Vectashield, Burlingame, CA, USA).

Confocal microscopy and analysis. Confocal fluorescence images were acquired on a Leica TCS SP5 scanning laser microscope (Leica, Buffalo Grove, IL, USA) using a $\times 40/1.25\text{NA}$ oil immersion objective to visualize the fiber placements and viral-mediated expression. Serial stack images covering a depth of 10 μm through multiple sections were acquired using equivalent settings. The Velocity image analysis software (Improvision/PerkinElmer, Waltham, MA, USA) was used for identifying co-localization of DAPI, eYFP and TH staining. Imaging and analysis were performed blind to experimental conditions.

Drug administration

Alpha-methyl-DL-p-tyrosine methyl ester hydrochloride (AMPT; Sigma-Aldrich, St. Louis, MO, USA; M3281) was prepared fresh in saline (0.9% NaCl, 10 mg ml^{-1}) and sterile filtered (0.2 μm) immediately prior to use. Adult male *Clock* $\Delta 19$ mice and WT littermates (24–36 weeks) were weighed and administered an intraperitoneal injection of AMPT (100 mg kg^{-1}) 60–90 min prior to behavioral testing. Control groups received an equal injection volume of sterile 0.9% NaCl. AMPT behavioral tests were separated by a minimum of 5 days. Daytime cohorts were administered AMPT within the time window of ZT5–9; nighttime cohorts received AMPT between ZT17–21.

Behavioral assays

Behavioral testing occurred between ZT6–10 (daytime cohorts) or ZT18–22 (nighttime cohorts). Mice were habituated to the testing room for 30 min prior to testing, unless otherwise specified.

Locomotor activity. Mice were individually placed into clear plexiglas chambers (KindsScientific Smart Cage Rack System; field dimensions: 9.5" \times 18.0") containing apparatus-embedded photobeams which measured horizontal locomotor activity for 60 min. Distance travelled was additionally measured in the open field and elevated plus maze (below) using Phenotracker video tracking software (www.tse-systems.com).

Elevated plus maze. The plus maze consisted of two plastic open arms perpendicular to two closed arms (arms: 30 \times 5 cm) and was elevated from the ground at a height of 60 cm. Mice were habituated to the testing room

for 30 min and then placed into the center of the plus-maze facing a closed arm and were allowed to explore the maze for 5 min. Behavior was video recorded and manually scored by a trained, blinded observer.

Open field. The open field consisted of a large 60 cm^3 plastic box. Mice were habituated to the testing room for 30 min and then individually placed into a corner in the periphery of the open field box and allowed to explore the arena for 15 min. The center was designated as a 20 cm^2 area in the center of the open field. Behavior was video-recorded and a trained blinded observer scored both time spent in, and entries into, the center of the arena.

Light/dark test. Anxiety-like behavior was assessed with a light/dark test using the KinderScientific Smart Cage Rack System interfaced to a PC running MotorMonitor software. Each chamber was equipped with a black Plexiglas box on one side of the chamber; a small doorway allowed free exploration of both dark and light chambers. Mice were initially habituated to the dark chamber for 2 min and then allowed free exploration of both light and dark chambers for the remainder of the 10 min test.

Forced swim test (FST). Mice underwent a single-day 6-min FST. Mice were habituated to the testing room for 30 min and then placed into a beaker filled with water (23–26 $^{\circ}\text{C}$; 20 cm depth). The time spent struggling, between 2 and 6 min, was measured by a blinded observer. Immobility was defined as all cessation of movement except those that were necessary to keep the animal afloat.

Tail suspension test. Depressive-like behavior was measured in optically stimulated mice using a 6-min tail suspension test. Mice were suspended by gently taping the entire extent of their tail, from the base to the tip, to a horizontally positioned 10 ml pipette situated over a large beaker. An observer blinded to treatment group recorded the total time spent struggling between 2 and 6 min.

Sucrose preference test. Mice were habituated for 3 days to a bottle containing a 1% sucrose solution that was placed in their homecage adjacent to a standard water bottle. The amount of water and sucrose solution consumed was measured daily and the % preference for sucrose relative to total fluid intake was calculated. The position of the bottles was balanced across groups to avoid potential side (left vs right) preferences. Daytime sucrose preference was measured on day 4 between ZT5 and 11; nighttime preference was measured between ZT16 and 23.

Gene expression

Animals were killed at six time points across the light/dark cycle (ZT 0, 4, 8, 12, 16, 20) and brains frozen on dry ice. VTA tissue was punched on a frozen stage from 300 μm slices taken on a cryostat (Leica). RNA isolation and cDNA synthesis was carried out as previously described.⁶ RNA was isolated using TRIzol reagent (Invitrogen) with remaining DNA digested using the DNA free system (Ambion, Austin, TX, USA). cDNA was synthesized with an oligo dT primer and superscript III reverse transcriptase enzyme (Invitrogen). Real-time PCR was performed in duplicate on the ABI 7500 Real-Time PCR system (Applied Biosystems, Carlsbad, CA, USA) using the Fast start SYBR green PCR master mix (Roche Applied Science, Indianapolis, IN, USA) with primers specific for *TH*, *Gapdh*, *Clock*, *Per2* and *Cryochrome 2* (*Cry2*) (see Supplementary Table). Relative levels of mRNA were calculated by the $2^{-\Delta\Delta\text{Ct}}$ method and normalized to corresponding *Gapdh* mRNA levels.¹⁹ Ct values represent the mean of two to five biological replicates of the same reaction.

SDS-PAGE and western blots

Mice were placed in a plexiglas restrainer and killed by microwave irradiation aimed at the head (5 kW, 1.2 s, Murimachi Kikai, Tokyo, Japan). VTA tissue was dissected from 1 to 2 mm slices with a 16-gauge tissue punch and immediately frozen for later use. For protein extraction, tissue samples were homogenized by sonication on wet ice in a buffer containing 320 mM sucrose, 5 mM HEPES, phosphatase inhibitor cocktail I and II (Sigma), protease inhibitor (Sigma), 5% SDS and 50 mM NaF. Protein homogenate was spun at 12 000 r.p.m. for 10 min at 4 $^{\circ}\text{C}$ and the supernatant carefully removed. DC assays (Bio-Rad, Hercules, CA, USA) were performed to quantitate protein levels. Aliquots of sample were combined in Laemmli SDS sample buffer (Bio-World, Dublin, OH, USA), and heated at 65 $^{\circ}\text{C}$ for 20 min. Samples were loaded (10 μg total protein per lane) and

run on a pre-cast 4–15% tris-glycine extended gel (Bio-Rad) at 100 V for ~90 min in 1 × TGS buffer (Bio-Rad). Proteins were transferred overnight at 4 °C onto Immobilon PVDF membranes (Millipore, Bedford, MA, USA) at 35 V in 1 × tris-glycine buffer. Membranes were re-wet briefly in a series of methanol, MilliQ water and 1 × PBS and blocked in Odyssey Blocking Buffer (LI-COR Biosciences, Lincoln, NE, USA) for 1 h at RT. Membranes were incubated overnight at RT with the following primary antibodies diluted in blocking buffer+0.2% Tween20: mouse anti-TH (1:2000, Sigma), rabbit anti-phospho-ser31 TH (1:400, Millipore), rabbit anti-phospho-ser40 TH (1:1000, Millipore) and mouse anti-GAPDH (1:20 000, Fitzgerald, Acton, MA, USA). Blots were stripped between application of the two rabbit phospho-antibodies and re-probed (NewBlot Stripping buffer, LI-COR Biosciences). Blots were washed in 1 × PBS+0.1% Tween20 and incubated for 1 h at RT with IRDye 680 conjugated goat anti-rabbit and IRDye 800 conjugated goat anti-mouse secondary antibodies (1:5000, LI-COR Biosciences) diluted in 0.2% Tween20+0.02% SDS. Blots were washed in 1 × PBS+0.1% Tween20 with a final wash in 1 × PBS. Blots were scanned using the Odyssey Infrared Imaging System (LI-COR Biosciences) interfaced to a PC running Odyssey 2.1 software for quantification. Values are expressed as a ratio to the corresponding GAPDH integrated intensity to control for potential discrepancies in amount of protein loaded. Values that were ± 1.5 standard deviations from the group mean were excluded from analyses.

Tissue L-DOPA high-performance liquid chromatography electrochemical detection analysis

Mice were injected with the amino acid decarboxylase inhibitor NSD-1015 (Sigma, 100 mg kg⁻¹, i.p.) and killed by cervical dislocation 60 min later. The nucleus accumbens and dorsal striatum were punched from separate tissue slabs using 2 mm diameter circular tissue punches (nucleus accumbens: +1.7–1.0; dorsal striatum: +1.0–0.0 mm, relative to bregma). Tissue punches were weighed and then frozen and stored at –80 °C until processing. Tissue was homogenized by sonication in 99 volumes (w/v) of ice-cold 100 mM HClO₄. Homogenate was centrifuged for 20 min at 15 000 g, 4 °C. Supernatants were recovered and passed through 0.2 µm filters and L-DOPA was quantified in the filtrates by high-performance liquid chromatography electrochemical detection. The high-performance liquid chromatography system consisted of a BASi (West Lafayette, IN, USA) LC-4C detector coupled to a BASi LCEC radial flow cell. Flow was provided by a Shimadzu (Columbia, MD, USA) LC-20AD solvent delivery module and preceded by an online degasser series 1100 from Agilent (Santa Clara, CA, USA). The chromatograms were analyzed using PowerChrom software (eDAQ, Colorado Springs, CO, USA). Monoamines in 10 µl tissue filtrate were separated on a 1 × 100 mm UniJet microbore 5 µm C-8 column (BASi). The mobile phase consisted of 24 mM Na₂HPO₄, 3 mM sodium octyl sulfate, 27.4 mM citric acid, 107 µM EDTA and 18.75% (v/v) MeOH, pH adjusted to 2.4 with NaOH. The flow was set at 50 µl min⁻¹ and the potential at +750 mV relative to an Ag/Cl reference electrode. Elution time for L-DOPA was 7 min.

Chromatin immunoprecipitation (ChIP)

ChIP assays were performed according to the methods described previously.²⁰ Briefly, 2 mm VTA containing midbrain dissections from C57BL/6 mice or *Clock*Δ19 mutant mice and their wild-type littermates were cross-linked with 1% formaldehyde for 15 min. Cross-linking was quenched with 2 M glycine for 5 min. The chromatin was sheared to 200–1000 bp fragments by eight rounds of sonication and cleared with Protein A beads (Thermo Scientific, Rockford, IL, USA). Between 60 and 100 µg of chromatin was used for each pull-down with 5–12 µg of each of the following rabbit primary antibodies: CLOCK-H276x (Santa Cruz Biotechnology, Santa Cruz, CA, USA); acetylated H3, (no. 06-599, Millipore); IgG (no. 12–370, Millipore) and anti-phospho-Creb s133 (no. 06-519, Millipore). Antibody–chromatin complexes were immunoprecipitated with Protein A beads according to the manufacturer's instructions. Following reverse cross-linking of input and precipitated samples, levels of protein binding at each promoter of interest were determined by measuring the amount of associated DNA by quantitative PCR (Applied Biosystems Prism 7700, Foster City, CA, USA) with primer sets for the TH proximal and distal site promoters (sequences are listed in Supplementary Table 1). Input DNA and immunoprecipitated DNA were amplified in duplicate in the presence of SYBR Green on the ABI 7500 Real-Time PCR system (Applied Biosystems, Carlsbad, CA, USA). Relative quantification of template DNA was performed using the fold enrichment method.

Luciferase assays

Plasmid construction. Wild-type and E-box mutant TH luciferase reporter gene constructs: The TH promoter reporter genes were prepared by inserting promoter fragments (containing the putative transcriptional start site) into the pGL3-luc vector. An initial TH promoter fragment (~1 kb) was generated by PCR from mouse genomic DNA with primers: 5'-TCCTGAA CCATTGCCTGAAGGAAG-3' upstream and 5'-GGTCCCAGTTCTGTCCA-3' downstream. This fragment was then inserted into pGEM-T Easy vector (cat. #A1360; Promega, Madison, WI, USA) and subsequently digested with *Eco*R1 to release the 1 kb promoter or *Sac*I and *Sal*I to liberate the 250 bp fragment. These were cloned into pGL3-luc to generate –1 kb and –250 bp reporter constructs. Mutagenic primers were designed to produce point mutations at the putative E-boxes of the TH-luc constructs. The proximal E-box sequence of the –250 TH luc construct was changed from CAGGTG to CCCGGG (this resulted in production of a diagnostic *Xmal* site), using complementary primers (coding sequence: 5'-CCCTTACATGG GGGCccgggAGAATGGGGCTGCC-3'). The distal E-box sequence of the –1 kb TH luc construct was changed from CAGCTG to CCCGGG (this resulted in a production of a diagnostic *Xmal* site), using complementary primers (coding sequence: 5'-CCCTTACATGGGGGccgggAGAATGGGG CTGCC-3'). The manufacturer's recommended protocol was followed for QuikChange II Site-Directed Mutagenesis (cat. # 200555; Agilent Technologies, Santa Clara, CA, USA) using a 6.5 min extension time. WT and mutant E-box TH-luc constructs were confirmed by DNA sequencing. CLOCK and CLOCKΔ19 expression plasmids: mouse Clock open reading frame was amplified by PCR from a cDNA kindly provided by J. Takahashi (UT Southwestern, Dallas, TX, USA), cloned in the pSG5 vector (Stratagene) with a FLAG epitope sequences at the 5' end. *Clock*Δ19 cDNA was generated by subcloning of full-length *Clock* cDNA into pGEX-4T-3 (GE Healthcare Bio-Sciences, Pittsburgh, PA, USA) for oligonucleotide-directed deletion of exon 19 with the U.S.E. Mutagenesis kit (Pharmacia Biotech). VP-16 CREB plasmids were kindly provided by E. Nestler (Mount Sinai School of Medicine, NY, USA).

Cell culture and luciferase assay. Rat pheochromocytoma (PC12) cells were cultured in Dulbecco's modified Eagle's Medium F-12 supplemented with 10% horse serum, 5% fetal bovine serum and 1% penicillin/streptomycin in a 37 °C, 5% CO₂ incubator. The assay was performed using PC12 cells transfected by electroporation (BTX 360) with 5 µg of either construct. For CLOCK/CLOCKΔ19 experiments, rat pheochromocytoma (PC12) cells were maintained in Dulbecco's modified Eagle's medium F-12, supplemented with 10% horse serum, 5% fetal bovine serum and 1% penicillin/streptomycin at 37 °C and 5% CO₂. Cells were plated in 12-well, collagen-coated plates at 80% confluence for 24 h before transfection. Cells were transfected by 3.5 µl Lipofectamine LTX (Invitrogen) according to the manufacturer's instructions with 5 µg TH-luc reporter plasmid, 1 µ or 10 µg CLOCK, 10 µg CLOCKΔ19 or 5 µg CREB expression plasmid, or a combination, depending on the experimental group. Empty vector plasmid (pCDNA) was used to normalize total amounts of DNA. After transfection, the cells were grown on 12-well collagen-coated dishes for 24 h before luciferase assays. Three days post transfection, cells were collected in lysis buffer and centrifuged to clear cellular debris. Thirty microliters of lysate was combined with 140 µl of luciferase assay buffer. Luminescence was measured using an FLx-800 microplate fluorescence reader after an automated injection of 40 µl of 1 mM luciferin per well. Luciferase activity was normalized to total protein levels.

Statistical analysis

Binary data were analyzed using an unpaired student's *t*-test while comparisons of three or more group means were conducted using an analysis of variance followed by a Bonferroni *post hoc* test. Analyses over time were conducted using a two-way repeated-measures analysis of variance followed by a Bonferroni *post hoc* test to control for multiple comparisons. Interactions that reached significance or trended towards significance were followed up with *post hoc* student's *t*-tests and are indicated in the corresponding figure legends. All datasets were tested for Gaussian distribution prior to analysis using the *F* test. Adequate sample size for each test was calculated by power analyses based on previous behavioral and molecular work. Where applicable, animals were randomly assigned to treatment groups through manual randomization, although care was taken to ensure that littermates were equally distributed among treatment groups. For behavioral assays, measurements that were ± 1.5 standard deviations from the group mean were excluded. Analyses were conducted using the GraphPad Prism 5 statistical software for Windows. The CircWave

v1.4 software (courtesy of Dr. Roelof Hut, <http://www.euclock.org/>) was used to analyze diurnal patterns of gene expression and protein levels. Data are presented as mean \pm s.e.m. with a two-tailed P -value ≤ 0.05 considered statistically significant. * $P \leq 0.05$, ** $P \leq 0.01$, *** $P \leq 0.001$, **** $P \leq 0.0001$. Significant treatment and time effects are denoted as # $P \leq 0.05$, ## $P \leq 0.01$, ### $P \leq 0.0001$.

RESULTS

Clock Δ 19 mice exhibit rapid mood-cycling across the light/dark cycle

Previously, we found that *Clock* Δ 19 mice exhibited a robust manic-like phenotype when tested during the daytime,³ however, we had yet to explore how behavior may change over the light/dark cycle. Consistent with previous findings,³ *Clock* Δ 19 mice exhibited reduced anxiety-related behavior during the daytime as indicated by increased exploration of the center of the open field (center entries, $P < 0.01$; center time, $P < 0.05$; Figure 1a) and light chamber of the light/dark box (light entries, $P < 0.05$; light time, $P < 0.05$; Figure 1b). *Clock* Δ 19 mice also exhibited an anti-depressive-like phenotype in the FST ($P < 0.0001$; Figure 1c) and sucrose-preference test ($P < 0.05$; Figure 1d), two well-validated behavioral assays that measure motivational and anhedonic facets of depressive-like behavior, respectively. Quite surprisingly, however, the behavioral profile of *Clock* Δ 19 mutant mice was time-dependent as manic-related behaviors were normalized to near wild-type (that is, euthymic-like) levels during the nighttime, resulting in a cyclic pattern in mood-related states over the light/dark cycle (night, mutant vs WT: open field, light/dark, and sucrose preference test, P 's > 0.05 ; mutant, day vs night: light/dark test, $P < 0.05$; FST, $P < 0.0001$; Figures 1a and d). To confirm that behavioral changes were not due to locomotor changes across the light/dark cycle (day vs night: WT, $P = 0.04$; mutants, $P < 0.05$; Supplementary Figure 1a), the data were re-analyzed to control for locomotor differences in the open field and light/dark test and yielded a consistent pattern of results (day, mutant vs WT: open field, $P < 0.01$; light/dark, $P < 0.05$; night, mutant vs WT: P 's > 0.05 ; Supplementary Figure 1b, c).

Daytime-specific increase in VTA dopamine activity in *Clock* Δ 19 mice

To determine how VTA dopamine cell firing changes over the course of the light/dark cycle in tandem with behavioral cycling, *in vivo* electrophysiological recordings were performed across the 24-h cycle. VTA dopamine neurons (WT: $n = 14/14/16/12$ and *Clock* Δ 19 mice: $n = 14/14/17/12$ for the number of dopaminergic neurons analyzed across each of the four time bins) were recorded during REM sleep to ensure locomotor activity would not influence dopaminergic firing (Supplementary Figure 2). In addition, neuronal firing was measured during REM sleep rather than anesthetization, as REM sleep is a normal physiological state.^{21,22} Consistent with previous reports,²³ *Clock* Δ 19 mice spent significantly less time in REM sleep during the day compared with WT littermates (ZT0–6, $P < 0.05$; ZT6–12, $P < 0.05$) and displayed a highly disrupted diurnal rhythm in overall REM sleep (Supplementary Figure 2). Firing rates were elevated in *Clock* Δ 19 mutants throughout the light/dark cycle, reaching significance at ZT0–6 ($P < 0.05$; Figure 2a). Bursting rates were also significantly elevated in *Clock* Δ 19 mice with the largest effect at ZT12–18 ($P < 0.05$; Figure 2b). As our data suggested that genotypic differences in bursting rate were largely driven by a reduced bursting rate in WT dopaminergic neurons, additional firing pattern analyses were performed. When bursting rates were compared in WT mice between ZT0–6 and ZT12–18, a significant reduction in bursting rate was found during the night (ZT0–6: 2.3 ± 0.4 bursts per 10 s; ZT12–18: 1.4 ± 0.3 bursts per 10 s) suggesting a diurnal rhythm in activity. Conversely, no differences in bursting rates were

observed in *Clock* Δ 19 mice, indicating a loss of diurnal rhythmicity. When differences in firing rate between day and night were compared, *Clock* Δ 19 mice displayed higher dopamine neuron firing during ZT0–6 (6.5 ± 1.1 Hz) than ZT12–18 (4.8 ± 0.4 Hz), with no differences detected in WT mice (ZT0–6: 3.4 ± 0.5 Hz; ZT12–18: 3.4 ± 0.4 Hz). These data demonstrate a significant daytime elevation in tonic dopaminergic activity and a loss in the diurnal rhythm of dopaminergic cell bursting in *Clock* Δ 19 mice.

As dopamine neural activity often parallels TH activity and dopamine synthesis,^{24–26} we measured TH transcript levels, markers of TH activity and dopamine synthesis in the VTA of WT and *Clock* Δ 19 across the light/dark cycle. Q-PCR analysis revealed that WT mice exhibited a significant diurnal variation in TH mRNA expression with low levels during the day and higher expression at night ($P = 0.0004$; Figure 2c). *Clock* Δ 19 mutant mice exhibited an overall increase in TH levels, with the greatest increase in expression observed during the day ($P < 0.05$; Figure 2c).

To determine whether increased TH gene expression results in altered TH protein levels, total TH protein and two of its phosphorylated forms, p-TH at Ser 40 and p-TH at Ser 31,²⁵ were measured in the VTA at four time points (day: ZT4, ZT9; night: ZT16, ZT21). The pattern of diurnal TH protein expression in WT mice was consistent with previous findings, demonstrating peak levels of TH during the day that decreased at night.²⁷ *Clock* Δ 19 mice exhibited a daytime-specific increase in total TH ($P < 0.01$; Figure 2d) and p-THser40/TH at ZT9 ($P < 0.05$; Figure 2e), representing a time slightly lagging the increase in TH mRNA expression. No differences in p-THser31/TH protein were found ($P > 0.05$; Figure 2f).

Dopamine synthesis assays were performed to determine whether increased TH activity in *Clock* Δ 19 mice leads to increased dopamine synthesis in the nucleus accumbens. High-performance liquid chromatography analysis revealed a 20% increase in dopamine synthesis in the NAc of *Clock* Δ 19 mice during the day with no difference detected at night ($P = 0.03$; Figure 2g). No significant alterations were found in the dorsal striatum ($P > 0.05$; Figure 2h), consistent with previous work showing no differences in TH protein levels in the substantia nigra of *Clock* Δ 19 mice.⁶

Chronic optic stimulation of VTA dopaminergic activity induces manic-like behavior

We next sought to determine whether daytime-specific increases in VTA dopamine firing are sufficient to reproduce manic-related behaviors. To accomplish this, we used optogenetic techniques to chronically manipulate VTA dopamine activity in TH::Cre mice. A chronic paradigm was employed to recapitulate the chronicity of increased daytime dopaminergic activity in *Clock* Δ 19 mice. Owing to the long-term nature of the stimulation paradigm employed, a double-mutated form of channelrhodopsin, the SSFO, ChR2(C128S/D156A), was used.¹⁵ The slower-off channel kinetics and enhanced sensitivity of SSFO offers the advantage that less frequent and intense stimulation is required to maintain a constant state of depolarization.¹⁵ To restrict opsin expression to midbrain dopamine neurons, a double-floxed inverted open reading frame (DIO) Cre-dependent virus, tagged with eYFP, was injected into the VTA of TH::Cre mice (Figures 3a and b). Specificity and efficiency of opsin expression, and accuracy of viral and optical fiber placement was confirmed *in vivo* (Supplementary Figures 3–6). cFOS immunohistochemistry was used as an indicator of neural activity and verified increased activity in SSFO-expressing VTA neurons following a single 5 s pulse of blue light (Supplementary Figure 7). Optrode recordings, which combine simultaneous optogenetic stimulation with electrophysiological recordings in awake behaving mice, additionally confirmed that a single 5 s pulse of blue light delivered every 15 min for 1 h (Figure 3c) increased dopamine neural firing concurrent with increased locomotor activity over the course of this stimulation

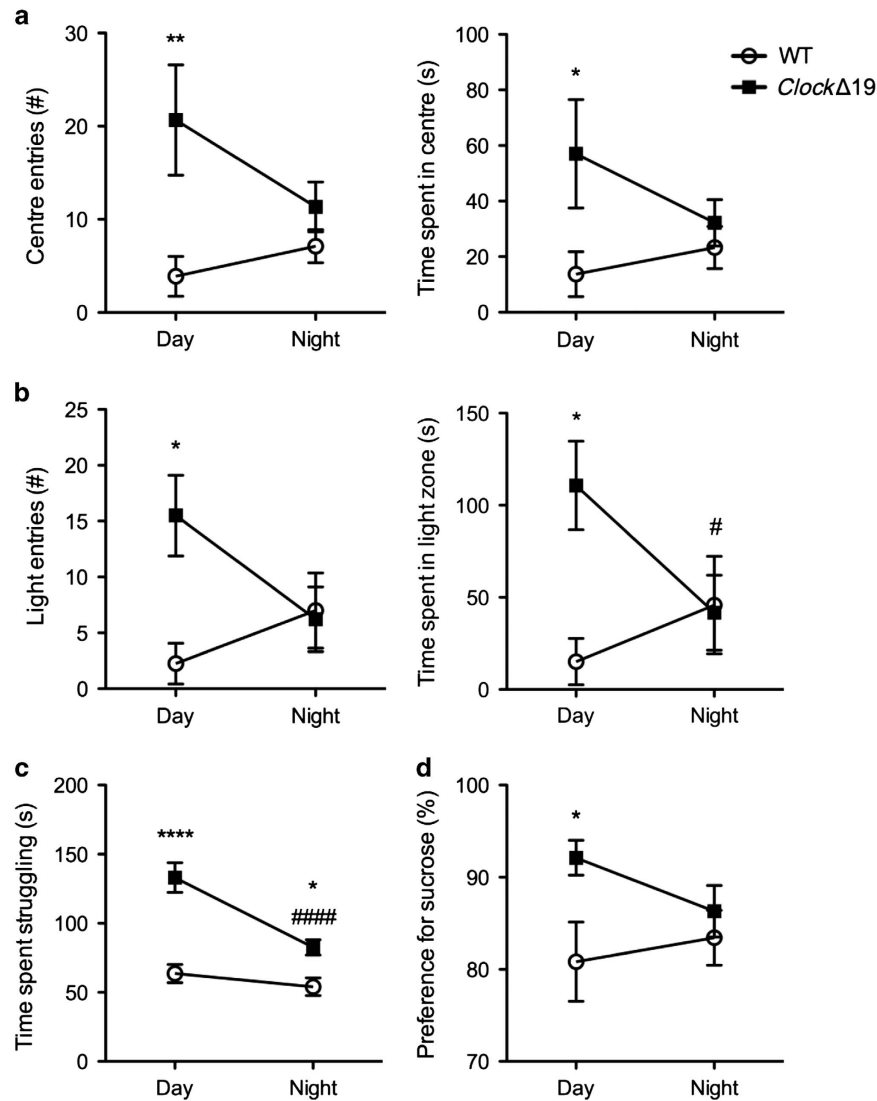


Figure 1. Behavioral mood-cycling across the light/dark cycle. Anxiety-like (a, b) and depressive-like (c, d) behaviors were measured during the day (ZT6–0) and night (ZT18–22) in wild-type (WT) and *ClockΔ19* mutant mice. (a) *ClockΔ19* mutant mice exhibited a significant increase in entries into the center of the open field during the day (main effect of genotype, $F_{1,28} = 11.72$, $P = 0.0019$; *post hoc*, $P < 0.01$) that decreased to WT levels at night (genotype by time interaction, $F_{1,28} = 4.19$, $P = 0.05$). *ClockΔ19* mice also spent more time in the center of the open field during the day (main effect of genotype, $F_{1,28} = 6.17$, $P = 0.02$; *post hoc*, $P < 0.05$) with differences no longer apparent at night. (b) This daytime-specific anxiolytic profile was also found in the light/dark test, where *ClockΔ19* mice entered the light chamber significantly more than WT controls during the day (main effect of genotype, $F_{1,28} = 4.23$, $P = 0.049$; *post hoc*, $P < 0.05$) but significantly decreased exploration to WT levels at night (genotype by time interaction, $F_{1,28} = 5.35$, $P = 0.03$; *post-hoc* student's *t*-test, $P = 0.06$, *ClockΔ19* day vs night). *ClockΔ19* mice also spent more time in the light chamber of the light/dark box during the day (main effect of genotype, $F_{1,28} = 4.29$, $P = 0.048$; *post hoc*, $P < 0.05$), with a significant decrease to WT levels at night (genotype by time interaction, $F_{1,28} = 5.03$, $P = 0.03$; *post hoc* student's *t*-test, $P = 0.049$, *ClockΔ19* day vs night). (c) *ClockΔ19* mice exhibited decreased depressive-like behaviors during the day as evidenced by increased struggling time in the forced swim test (main effect of genotype, $F_{1,28} = 44.7$, $P < 0.0001$; *post hoc*, $P < 0.0001$) and (d) an increased preference for a 1% sucrose solution (main effect of genotype $F_{1,27} = 5.46$, $P = 0.027$; *post hoc*, $P < 0.05$). Differences in depressive-like behaviors were no longer evident at night as *ClockΔ19* mutant mice significantly decreased struggling time to near WT levels in the forced swim test (c): genotype by time interaction, $F_{1,28} = 7.84$, $P = 0.0092$; *post hoc*, $P < 0.0001$) and no longer showed a preference for sucrose relative to WT mice (d). Day and night cohorts, $n = 8–9$ per group.

period, with a peak in both neural and locomotor activity occurring 15–30 min following stimulation ($P < 0.05$; Figure 3d). This acute stimulation-induced hyperactivity was most pronounced on day 7, following 6 days of stimulation (Supplementary Figure 8). Indeed, six successive days of stimulation (1 h per day) were required before a change in baseline locomotor activity was observed ($P < 0.05$; Supplementary Figure 8). Similarly, *in vivo* recordings confirmed that chronic optic stimulation led to a

sustained increase in baseline VTA dopamine firing on day 8, independent of any further stimulation (Figure 3e).

Once this timeline was established, a unique stimulation paradigm was used whereby mice received seven successive days of 1 h per day optogenetic stimulation prior to behavioral testing. To control for the diurnal specificity of neural firing observed in *ClockΔ19* mice, TH::Cre mice were optically stimulated during the day, when VTA dopamine cell firing is high in *ClockΔ19* mice.

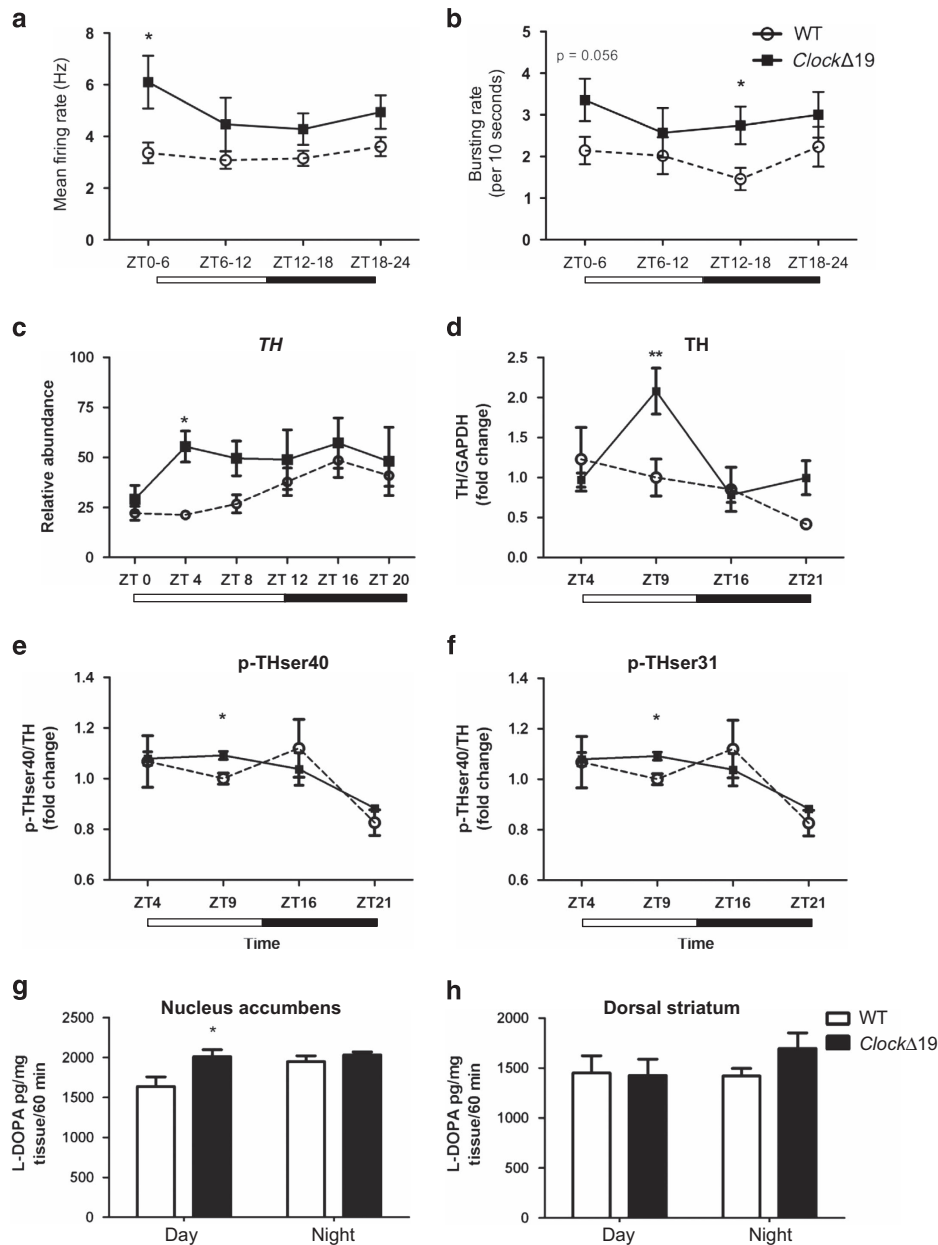


Figure 2. Time-specific alterations in VTA dopaminergic activity in *ClockΔ19* mice. **(a)** Two-way analysis of variance of firing rate found a significant genotype effect ($F_{1,112} = 12.67$, $P = 0.0006$). *Post hoc* tests revealed significant differences in the firing rate of dopaminergic neurons during the first 6 h of the light cycle and the last 6 h of the dark cycle ($P < 0.05$ using student's *t*-test; $n = 14/14/16/12$ and $14/14/17/12$ for the number of dopaminergic neurons analyzed in WT ($n = 8$) and *ClockΔ19* mice ($n = 9$), respectively). **(b)** Two-way analysis of variance of bursting rate found a significant genotype effect ($F_{1,112} = 8.6$, $P = 0.004$) with *post hoc* analyses revealing significant differences in the bursting rate of dopaminergic neurons during the first 6 h of the dark cycle ($P < 0.05$, by student's *t*-test; $n = 14/14/16/12$ and $14/14/17/12$ for the number of dopaminergic neurons analyzed in WT and *ClockΔ19* mice, respectively). **(c)** Relative abundance of TH mRNA normalized to the expression of *Gapdh*. Two-way analysis of variance revealed a significant genotype effect ($F_{1,45} = 9.42$, $P = 0.004$) with a specific increase in TH expression at ZT4 in *ClockΔ19* mice ($P < 0.05$, $n = 3-5$ animals per genotype per time point). Diurnal variation was significant in wild-type (WT) mice (CircWave: $F_{2,27} = 10.63$, $P = 0.0004$) but not in *ClockΔ19* mutants ($P > 0.05$). **(d)** A significant main effect of time was found for total TH ($F_{3,28} = 5.34$, $P = 0.005$), with an increase in *ClockΔ19* mouse TH levels at ZT9 ($P < 0.01$). Diurnal variation was statistically significant in mutants (CircWave: $F_{2,17} = 5.15$, $P = 0.02$). **(e)** There was a significant effect of time on phosphorylated TH (ser 40) protein ($F_{3,32} = 6.50$, $P = 0.002$), with *ClockΔ19* mice exhibiting a specific increase in THser40 levels at ZT9 ($P < 0.05$, student's *t*-test). Diurnal variation in THser40 was statistically significant in mutants (Circwave: $F_{2,17} = 7.18$, $P = 0.005$). **(f)** No differences in phosphorylated THser31 protein levels were found at any time point measured. Inset depicts average protein levels over 24 h. **(e, f)** Dopamine synthesis assay. **(g)** Dopamine synthesis was significantly increased in *ClockΔ19* mutant mice as measured by L-Dopa in the nucleus accumbens after NSD-1015 administration during the light phase, at ZT4 ($t_9 = 2.546$, $P = 0.03$). **(h)** Dopamine synthesis was unaltered in the dorsal striatum of *ClockΔ19* mutants ($P > 0.05$, $n = 5-8$ per group; dark phase = ZT16). White and dark bars below graph represent daytime and nighttime measurements, respectively.

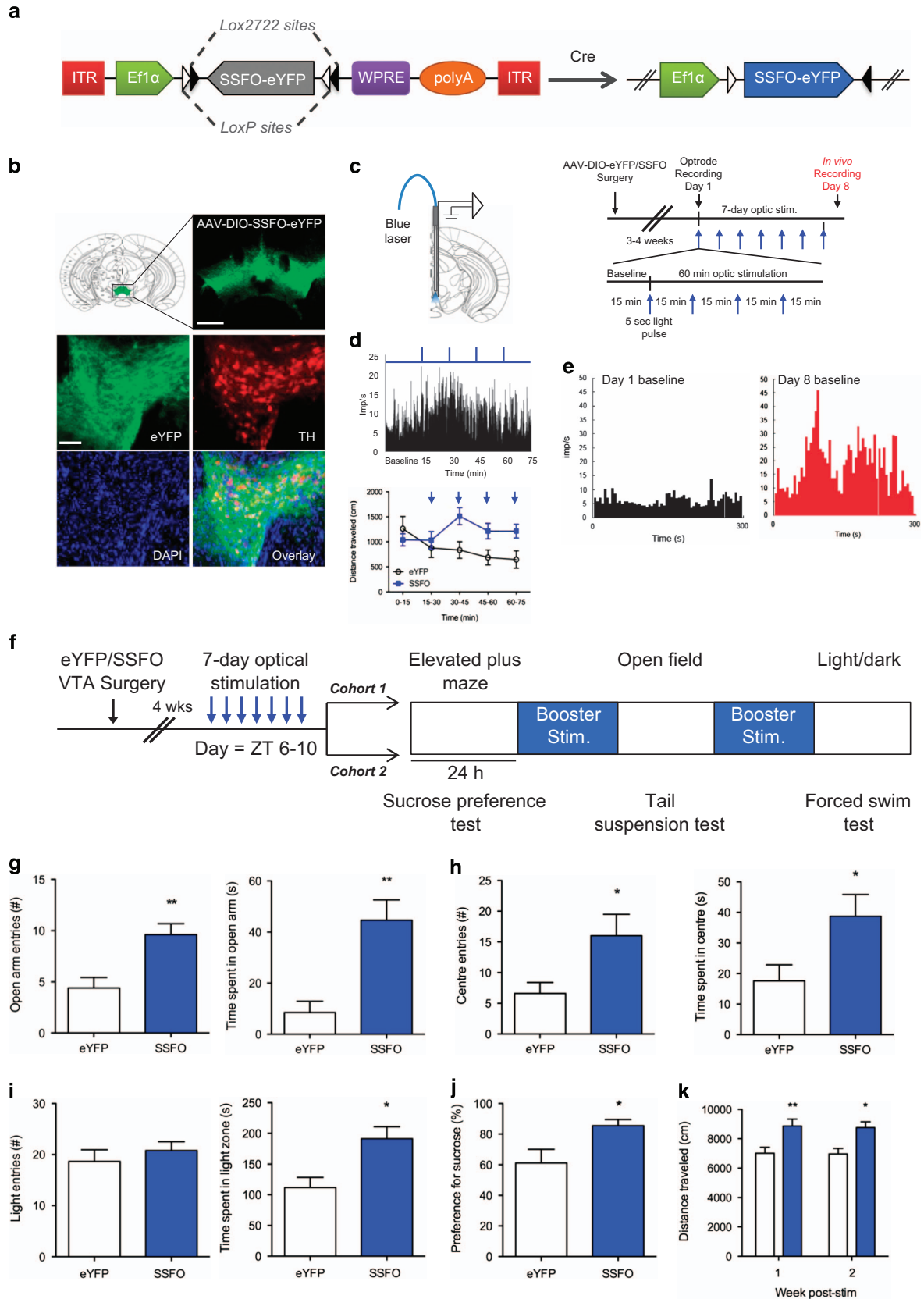


Figure 3. Effect of chronic VTA optical stimulation on manic-related behaviors. **(a)** Schematic of the Cre-dependent stable step function opsin (SSFO) viral construct tagged with enhanced yellow fluorescent protein (eYFP) used for long-term optical control of neural activity. Two incompatible LoxP sites surround a double-inverted open reading frame that ensures specificity of viral transduction and SSFO expression in cre-containing cells. **(b)** Expression of SSFO (AAV5-ChR2(C128S/D156A)-eYFP) in the ventral tegmental area (VTA) of a tyrosine hydroxylase (TH)::Cre mouse showing specificity of SSFO expression (green) in TH+ cells (red). TH::Cre mice lacking cre-recombinase (-/-) were used as a negative control and showed no viral expression in TH+ cells (data not shown). Scale bar: 4x = 500 μm; 20x = 100 μm. **(c)** Left panel: Schematic of unilateral optrode implantation for simultaneous optic stimulation and electrophysiological recording of VTA dopamine neurons. Right panel: Chronic stimulation paradigm: 3–4 weeks following surgery, mice received 7 days of optic stimulation. On each day, mice were given a 5 s pulse of 473nm or 447 nm light every 15 min for a total of 60 min. Electrophysiological recordings were conducted in a separate cohort of mice that underwent the chronic stimulation paradigm whereby VTA DA recordings were performed in awake behaving mice on day 1 and again on day 8 for comparison. **(d)** Top panel: Single neuron recording on day 1 of the stimulation paradigm in an SSFO-mouse confirmed increased VTA dopamine neural firing during the 5 s light pulse and a sustained increase in firing over the 60 min stimulation paradigm (blue lines atop graph represent single 5 s pulses of blue light delivered 15 min apart). Bottom panel: 1 h optic stimulation of the VTA in SSFO-mice increased locomotor activity throughout the course of stimulation (main effect of treatment: $F_{1,60} = 5.84$, $P = 0.019$), with a significant peak in activity occurring 15–30 min ($P < 0.05$) after the start of stimulation (first stimulation occurred at the 15 min mark) **(e)** Representative 5 min baseline (that is, independent of concurrent optic stimulation) *in vivo* recording from an awake freely moving TH::Cre mouse expressing SSFO confirmed that 7 days of optic stimulation (as depicted above in Figure 3c, right panel) increased the mean baseline firing rate of VTA dopamine neurons on day 8 (red trace) compared with day 1 (black trace). Firing rates were averaged across 5 s time bins. **(f)** Chronic optical stimulation paradigm for behavioral testing: 4 weeks following viral-mediated delivery of SSFO or eYFP to the VTA, TH::Cre mice were optically stimulated with 473nm or 447 nm light for 1 h per day for 7 days within the ZT6–10 time window, followed by behavioral testing to assess anxiety-related (cohort 1) and depressive-related (cohort 2) behaviors. Behavioral tests were separated by 48 h with a 'booster' optical stimulation given between test days to sustain alterations in VTA dopamine neural activity. Note that mice did not receive optical stimulation on the day of behavioral testing. **(g–i)** TH::Cre mice that received chronic optical stimulation exhibited significantly decreased anxiety-related behavior as evident by increased entries into, and time spent in, **(g)** the open arms of the elevated plus maze (entries: $t_8 = 3.49$, $P = 0.008$; time: $t_8 = 4.3$, $P = 0.003$), **(h)** center of the open field (entries: $t_7 = 2.55$, $P = 0.038$; time: $t_7 = 2.42$, $P = 0.046$) and **(i)** light chamber of the light/dark box (entries: $P > 0.05$; time: $t_6 = 3.12$, $P = 0.021$). **(j)** Chronic optical stimulation increased sucrose preference in mice expressing SSFO ($t_{10} = 2.86$, $P = 0.017$). **(k)** Two-way repeated measures analysis of variance revealed a main effect of group ($F_{1,14} = 13.46$, $P = 0.0025$) whereby 7 days of chronic optic stimulation lead to a persistent and sustained increase in baseline locomotor activity at both 1 ($P < 0.01$) and 2 weeks ($P < 0.05$) after cessation of optogenetic stimulation. For behavioral experiments, cohort 1: $n = 5–6$ per treatment group; cohort 2, $n = 5–9$ per group.

Following completion of 7 days of optic stimulation, mice were tested in a behavioral battery to assess features of manic-like behavior, including locomotor, anxiety- and depressive-like behaviors (Figure 3f).

SSFO-mice explored the open arms of the elevated plus maze (entries, $P = 0.008$; time, $P = 0.003$; Figure 3g), center of the open field arena (entries, $P = 0.038$; time, $P = 0.046$; Figure 3h) and light chamber of a light/dark box (time, $P = 0.021$; Figure 3i) more than eYFP controls, indicating anxiolysis, or increased exploratory and risk-taking behavior. As SSFO mice exhibited hyperactivity during behavioral testing (elevated plus maze, $P < 0.05$; light/dark, $P < 0.01$; Supplementary Figure 9), percent distance traveled was additionally used as a read-out of anxiety-like behavior to avoid potential confounds of hyperactivity on locomotor-based exploratory measures; the results were consistent with those reported above. Both the anhedonic and motivational features of depressive-like behavior were assayed using the sucrose preference test, to measure reward behavior, and the tail suspension and FSTs to measure motivation to escape an inescapable paradigm. SSFO-mice exhibited an increased preference for sucrose following 7 days of chronic stimulation ($P = 0.017$; Figure 3j). Conversely, chronic enhancement of VTA dopamine activity had no impact on depressive-like measures in the tail suspension test or FST ($P > 0.05$; Supplementary Figure 9a and b). Notably, behavioral changes in response to chronic stimulation persisted for up to 2 weeks following cessation of optic stimulation (week 1, $P < 0.01$; week 2, $P < 0.05$; Figure 3k).

CLOCK binds the TH promoter in the VTA

To determine whether increased VTA dopamine levels and activity in *ClockΔ19* mice result from CLOCK acting as a direct transcriptional regulator of TH, we first characterized the transcript profile of *Clock* over the light/dark cycle. Interestingly, *Clock* gene expression was anti-phasic to TH expression in WT mice, with a peak occurring during the light phase, when TH expression is lowest, and a trough during the dark phase when TH expression was highest (Supplementary Figure 10a). To ensure that CLOCK

maintains its function as a transcriptional activator in brain regions outside of the suprachiasmatic nucleus, two well-established downstream targets of suprachiasmatic nucleus CLOCK transcriptional activation were measured in the VTA. As expected,²⁸ VTA *Per2* and *Cry2* expression were decreased in *ClockΔ19* mice, confirming that CLOCK can act as a transcriptional activator at gene targets external to the suprachiasmatic nucleus (*Per2*, $P < 0.001$; *Cry2*, $P < 0.001$; Supplementary Figure 10b and c).

We next determined the ability of CLOCK to directly bind E-box elements in the TH promoter (CANNTG) by performing ChIP assays on VTA-containing midbrain tissue. Two primer sets were created to amplify distal and proximal regions of the promoter containing putative E-Boxes (Supplementary Table 1; Supplementary Figure 11). ChIP analyses were performed on C57BL/6 mice at four time points: daytime = ZT4 and ZT9 and nighttime = ZT16 and ZT21. CLOCK was present at both TH promoter sites during the day (distal: Figure 4a; proximal: Figure 4c), with no enrichment observed above background at night. CLOCK binding was then assessed in *ClockΔ19* mutants during the day at ZT4, when binding is expected based on the results in Figures 4a and c. Consistent with the WT data, the *CLOCKΔ19* mutated protein was enriched at both TH promoter sites in *ClockΔ19* mice (distal: Figure 4e; proximal: Figure 4f). These data indicate that the mutated CLOCK protein is capable of binding DNA, however, the missing exon 19 appears critical for conferring proper transcriptional regulation. To test the functional significance of CLOCK binding at the TH promoter, we interfered with CLOCK's ability to properly bind TH. Luciferase assays were performed with TH-luc reporter plasmids containing either an intact or mutated E-box. Disruption of CLOCK binding through mutation of either E-box site significantly increased TH-luc reporter activity (proximal, $P < 0.0001$ and distal, $P < 0.01$; Figure 4g), demonstrating that the repression of TH transcription is E-box-dependent.

We hypothesized that phosphorylated cAMP Response Element Binding Protein (p-CREB) may compete with CLOCK for binding at the proximal TH promoter given the proximity of the CRE-binding site upstream of the proximal CLOCK E-box-binding site (Supplementary Figure 11) and the well-established role of CREB

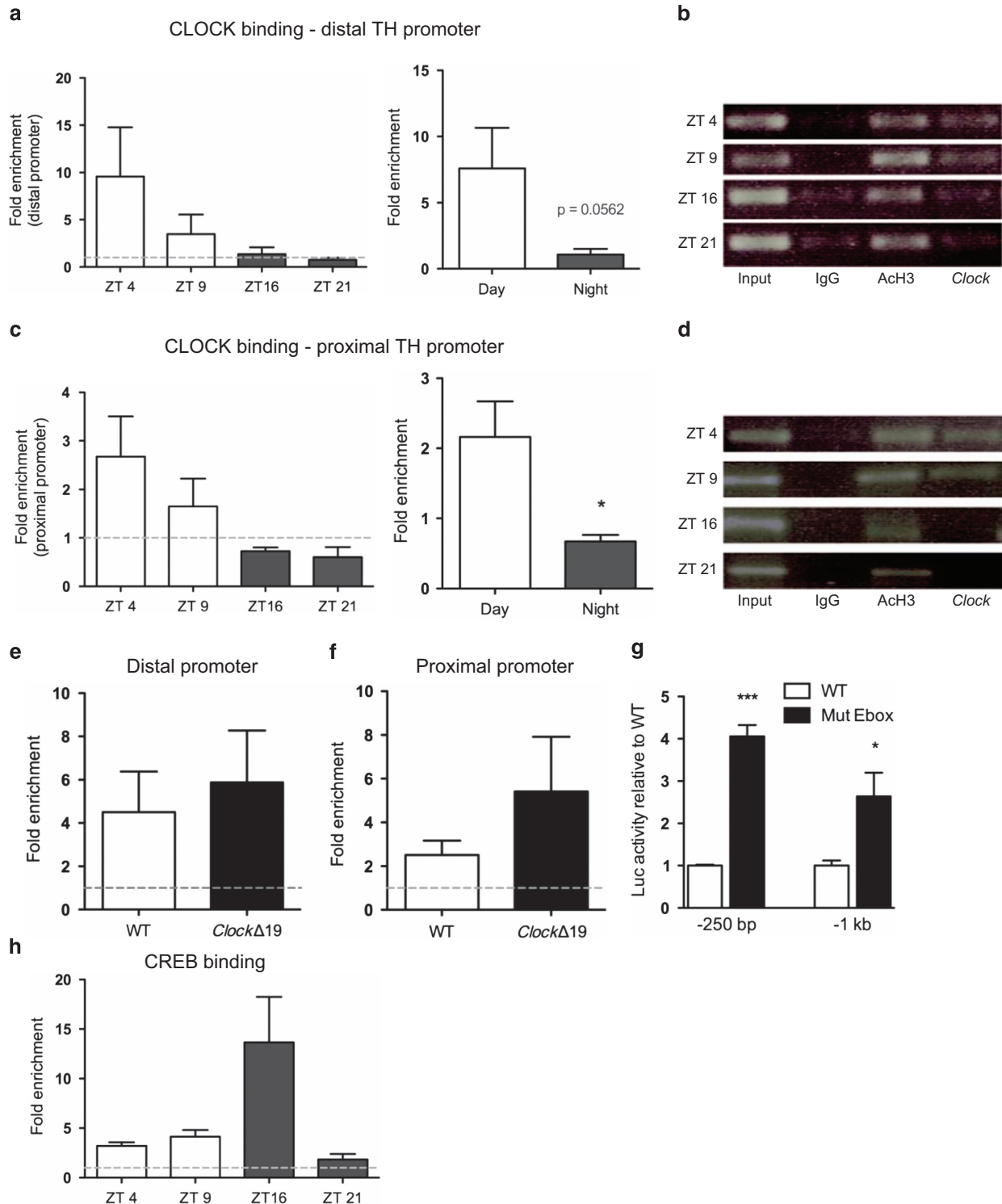


Figure 4. CLOCK binding at the *TH* promoter. **(a)** Fold enrichment, as calculated from Ct values, at distal promoter region across ZT time following chromatin immunoprecipitation with a CLOCK-specific antibody in C57BL/6 mice ($n = 3-4$ per time point). **(a)**, right) Comparison of CLOCK binding at the distal *TH* promoter during the light (averaged values of ZT4 and ZT9 from graph, left) versus dark phase (averaged values of ZT16 and ZT21 from graph, left) shows a strong trend toward a diurnal variation in promoter occupancy ($t_{13} = 2.113$, $P = 0.056$). **(b)** Representative agarose gels of q-PCR products from ChIP assay for graphs in **(a)**. **(c)** Binding at the proximal *TH* promoter. **(c)**, right) Significant diurnal variation in CLOCK occupancy of the *TH* proximal promoter ($t_{13} = 2.713$, $P = 0.02$). **(d)** Representative agarose gels of q-PCR products from ChIP assay for graphs in **(b)**. **(e, f)** Fold enrichment at distal **(e)** and proximal promoter region **(f)** following ChIP with a CLOCK-specific antibody comparing *Clock*Δ19 mutants to wild-type (WT) controls; ($n = 4-6$ per time point). **(g)** Relative luciferase activity in PC12 cells transfected with WT *TH*-luc constructs (250 bp or 1000 bp) or *TH*-luc constructs containing mutant E-boxes. Mutating the E-boxes significantly increased luciferase activity at the proximal ($t_{16} = 11.30$, $P < 0.0001$) and distal site ($t_9 = 3.158$, $P < 0.01$). **(h)** Differential levels of p-CREB(s133) binding at the proximal *TH* promoter across ZT time with increased binding observed during the beginning of the dark phase (ZT16) in C57BL/6 mice.

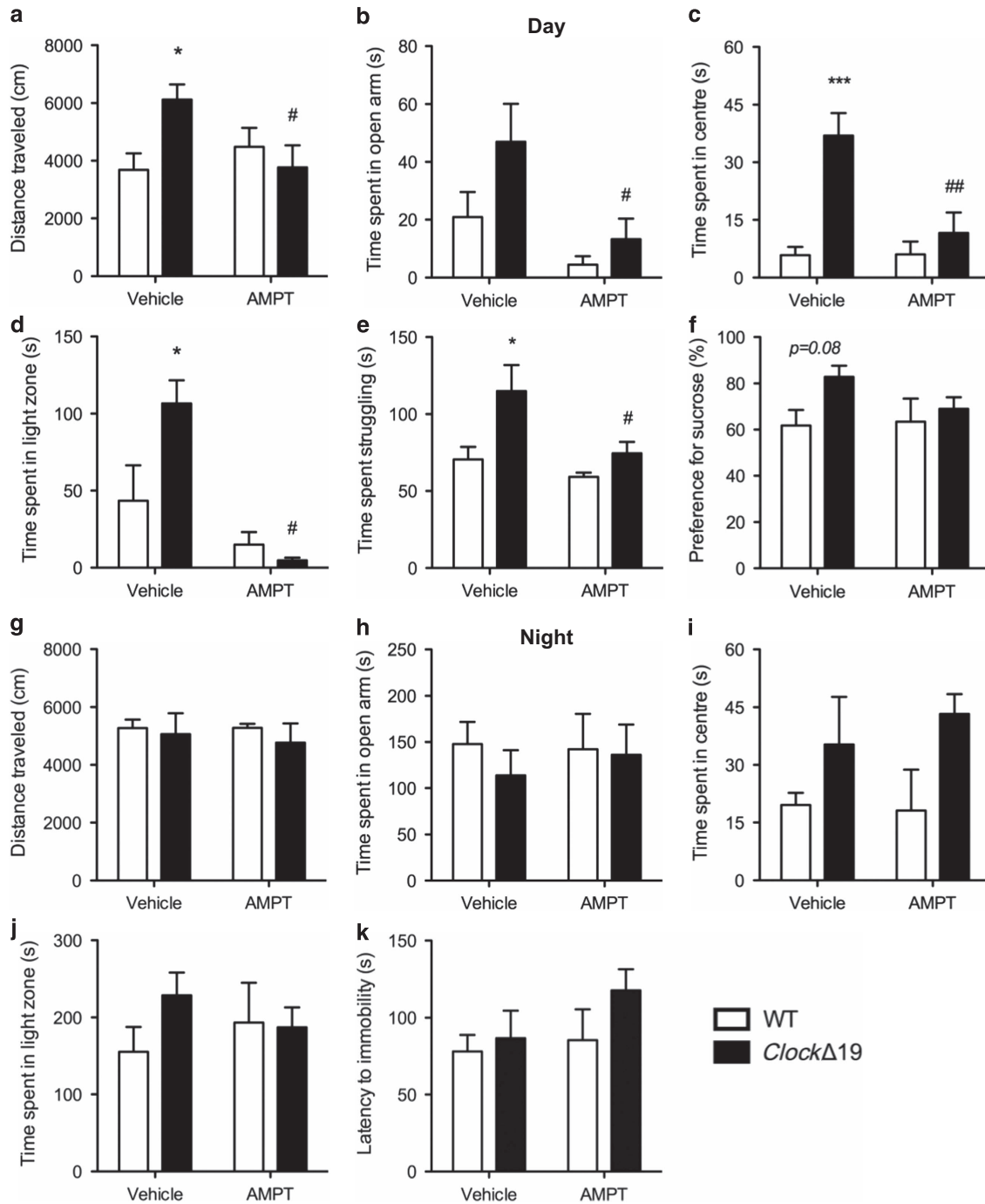


Figure 5. Daytime-specific tyrosine hydroxylase inhibition reverses manic-like behaviors. *Clock*Δ19 mice and wild-type (WT) littermates received an intraperitoneal injection of either 0.9% saline (vehicle) or AMPT (100 mg kg⁻¹) during the day (ZT6–10) or night (ZT18–22) and were tested for anxiety- and depressive-related behaviors 60–90 min later. Daytime cohorts (a–f): (a) Two-way analysis of variance revealed a significant interaction of genotype and treatment ($F_{1,20} = 6.66, P = 0.01$) on distance traveled in a novel environment where vehicle-treated *Clock*Δ19 mice exhibited hyperactivity ($P < 0.05$) which decreased to WT levels following AMPT treatment ($P < 0.05$). Vehicle-treated *Clock*Δ19 mice also showed the expected decrease in anxiety-like behavior compared with vehicle-treated WT littermates as indicated by increased exploration of the aversive open arms of the elevated plus maze (main effect of genotype: $F_{1,20} = 5.09, P = 0.03$), (c) center of the open field (main effect of genotype: $F_{1,15} = 16.22, P = 0.001$; *post hoc* $P < 0.001$), and (d) light chamber of the light/dark box (interaction between genotype and treatment: $F_{1,15} = 6.12, P = 0.03$; *post hoc* $P < 0.05$ for vehicle treated groups) and displayed (e, f) decreased depressive-like behavior in the forced swim test (e) as indicated by increased time spent struggling ($F_{1,16} = 8.73, P = 0.009$; *post hoc* $P < 0.05$) and an increased preference for sucrose (f) in the sucrose preference test (genotype effect: $F_{1,25} = 3.24, P = 0.08$). Importantly, AMPT treatment significantly reversed *Clock*Δ19 mice manic-behavioral features to WT levels (a–e). Main effect of treatment in (a) reported above; (b) $F_{1,20} = 10.48, P = 0.004$, *post hoc* $P < 0.05$; (c) $F_{1,15} = 7.6, P = 0.01$, *post hoc* $P < 0.001$; (d) $F_{1,15} = 19.18, P = 0.0005$, *post hoc* $P < 0.001$; (e) $F_{1,16} = 6.55, P = 0.02$, *post hoc* $P < 0.05$. (g–k) Nighttime cohorts. Vehicle-treated *Clock*Δ19 mice did not exhibit manic-related behavioral features when tested at night, nor did AMPT treatment affect behavior in *Clock*Δ19 mice or WT littermates. Daytime cohorts, $n = 5–6$ per group; Daytime sucrose preference test and nighttime light/dark test, $n = 7/8$; Nighttime cohorts, $n = 5–8$ per group.

in the regulation of *TH* transcription.²⁹ Indeed, an increase in p-CREB binding was found at the *TH* proximal promoter site during the night relative to the day that represents an opposite pattern of binding from that of CLOCK at the *TH* promoter (Figure 4h). This suggests an antagonistic relationship between CLOCK and p-CREB in regulating *TH* transcription.

Daytime TH inhibition reverses manic-like behaviors

Finally, we sought to determine whether daytime increases in TH activity are necessary to produce a switch to a manic-like state in *ClockΔ19* mice through direct pharmacological inhibition of TH activity. Mice were administered AMPT either during the day, at a time corresponding to peak levels of dopaminergic activity in *ClockΔ19* mice, or during the dark phase when no difference in dopaminergic activity is observed. As expected, vehicle-treated *ClockΔ19* mice exhibited a hyperactive phenotype ($P < 0.05$; Figure 5a) and an overall anxiolytic behavioral profile compared with WT mice during the daytime as characterized by increased exploration of the open arms of the elevated plus maze (main effect of genotype, $P = 0.03$; Figure 5b), center of the open field ($P < 0.001$; Figure 5c) and light chamber of the light/dark test ($P < 0.05$; Figure 5d). *ClockΔ19* mice also exhibited an anti-depressive phenotype during the daytime as demonstrated by increased time spent struggling in the FST ($P < 0.05$; Figure 5e) and an increased preference for sucrose (main effect of genotype, $P = 0.08$; Figure 5f). Importantly, all behavioral components of the *ClockΔ19* mouse manic-like phenotype were reversed to WT levels with daytime AMPT treatment (P 's < 0.05 , vehicle vs AMPT; Figures 5a and e). AMPT did not alter general locomotor activity ($P > 0.05$; Supplementary Figure 12a,b) except in the light/dark test where it decreased overall distance traveled in *ClockΔ19* mice ($P < 0.01$; Supplementary Figure 12c). In this case, data were also plotted as % distance traveled and yielded similar results to those reported above ($P < 0.01$; Supplementary Figure 12d). Conversely, AMPT had no behavioral effects when administered during the dark phase (P 's > 0.05 , vehicle vs AMPT; Figure 5g and k and Supplementary Figure 12e and g), when *ClockΔ19* mice were found to be in a euthymic-like state.

DISCUSSION

The current study demonstrates that disrupted function of the circadian protein, CLOCK, by the $\Delta 19$ mutation leads to rapid mood-cycling across the light/dark cycle. To the best of our knowledge, this is the first mouse model that spontaneously switches between two different mood-related states. This behavioral cycling between daytime manic-like behavior and nighttime euthymic-like behavior coincided with time-dependent changes in VTA dopamine neuronal firing and TH activity across the light/dark cycle. Specifically, changes in TH activity were determined by measuring the levels of transcript, markers of protein activity and dopamine synthesis. Levels of phosphorylated ser40, and not ser31, were increased in *ClockΔ19* mice. Phosphorylation at the serine 40 residue, and to a lesser extent, at the serine 31 residue of the TH protein increases TH activity and catecholamine synthesis *in vivo*.²⁴ Although phosphorylation at ser40 and ser31 occur in response to a multitude of acute stimuli,³⁰ sustained increases in phosphorylation at ser40 are indicative of chronic changes in TH activity³¹ and are known to parallel changes in dopamine synthesis. Furthermore, changes in TH expression and phosphorylated ser40 are known to correlate with dopamine neuron activity and depolarization.^{24,26} The increases in TH activity and dopamine synthesis found here coincided with the daytime increase in VTA dopamine neuronal firing observed in *ClockΔ19* mice, suggesting that increased TH activity and dopamine synthesis may act as a precursor or consequence of increased neural firing.

Using a novel optogenetic stimulation paradigm, we demonstrate that chronic stimulation of daytime VTA dopaminergic neurons is sufficient to increase daytime exploratory and reward-related behaviors in WT mice. This behavioral profile is similar to that observed in *ClockΔ19* mice, suggesting that chronically increased VTA dopamine neural firing may underlie specific components of the *ClockΔ19* mouse manic-like behavioral phenotype. Indeed, tonic but not phasic^{21,22} activation of VTA-DA neurons in mice has been shown to produce an anxiolytic response,³² which is consistent with current findings and suggests that changes to tonic DA firing underlie anxiety-like behavioral responses. Previous work from our group has found that a selective reduction in VTA neuronal firing in *ClockΔ19* mice normalizes their anxiety-like, but not depressive-like behaviors.⁷ Interestingly, chronic optic stimulation of VTA dopamine neurons had no impact on depressive-like behavior as measured in the tail suspension and FSTs. However, other studies have found that acute VTA optogenetic modulation decreases depressive-like behavior induced by stressors.^{33,34} This highlights the complexity of the behaviors and neural circuits under investigation but may also reflect the properties of the different opsins used to modulate neural activity and their physiological effects on neural firing. For instance, the step-function opsins used in the current study do not drive synchronous trains of neural firing in response to light, as channelrhodopsins do, but rather enable step-like control of membrane potential by bringing neurons closer to action potential threshold.^{35,36} This creates an UP state and can be considered a more physiologically relevant approach to neural circuit manipulation.³⁶ Indeed, the chronic stimulation paradigm introduced here lead to a persistent and sustained change in behavior following cessation of all optogenetic stimulation suggesting that the stimulation paradigm altered the physiological properties of VTA dopamine neurons and/or downstream neural circuits without the need for additional circuit modulation. The plastic changes induced by this paradigm and the longevity of the effect will be an interesting avenue of investigation for future studies.

This is the first study to report that the circadian protein, CLOCK, can directly regulate *TH*. This finding is surprising given that most studies have reported that CLOCK acts as a transcriptional activator at CLOCK-controlled gene promoters, rather than as a suppressor.³⁷ Conversely, CREB (a known activator of TH expression) binding to the TH promoter occurred in an opposite diurnal pattern to CLOCK, suggesting an antagonistic relationship between CLOCK and CREB in *TH* regulation. Importantly, we show that the *CLOCKΔ19*-mutated protein is still capable of binding DNA. This integral finding has been confirmed in a recent study which demonstrated that the *CLOCKΔ19*-mutated protein binds DNA, albeit with lower affinity to E-box regulatory sites, resulting in reduced transcriptional efficiency.³⁸ In light of the current findings, this would suggest that the *CLOCKΔ19* protein is a less effective transcriptional repressor of *TH* and provides an additional mechanistic explanation for the increased TH activity observed in *ClockΔ19* mice. The importance of CLOCK in the regulation of TH is evolutionarily conserved as fruit flies with a mutation in the *Clock* gene also have an increase in TH expression.³⁹ Interestingly, a recent study found that another circadian protein, REV-ERBa, also directly regulates the expression of *TH* in dopamine neurons and that inhibition of REV-ERBa can lead to a very similar manic-like profile and a hyperdopaminergic state.⁴⁰ These results provide further confirmation of the important role of circadian genes in the regulation of dopamine synthesis and the precipitation of mania.

The importance of this increased TH activity to manic-like symptoms was demonstrated by the complete reversal of manic-related behaviors in *ClockΔ19* mice following TH inhibition during the day. Both anxiety- and depressive-like features were reversed in *ClockΔ19* mice by daytime AMPT treatment whereas VTA optic stimulation in TH::Cre mice reproduced only the anxiolytic and

rewarding features of the *Clock* Δ 19 mouse manic-like phenotype. In this respect, AMPT-induced TH inhibition likely targets multiple brain regions, whereas optic stimulation specifically targeted the VTA. Such circuit-specific functional differences will be interesting to explore in future studies.

CONCLUSIONS

The current study uncovers a novel mechanism for regulation of TH by CLOCK and underscores the importance of normal patterns of dopaminergic activity in the proper regulation of mood-related behaviors. This has far-reaching implications for bipolar disorder and other psychiatric disorders, where the inability to regulate mood is a central defining feature. Given the paucity of effective treatment options for bipolar disorder,^{41–43} the current findings represent a novel therapeutic avenue and extend to a multitude of diseases that involve dysfunction in limbic dopaminergic circuitry. Furthermore, the use of optogenetic technology with step function opsins opens the door for future studies to examine the effects of chronic stimulation of multiple neurotransmitter systems across various brain regions to determine the impact on complex behavioral phenotypes.

CONFLICT OF INTEREST

The authors declare no conflict of interest.

ACKNOWLEDGMENTS

This work was supported by funding from the McKnight Foundation, the National Alliance for Research on Schizophrenia and Depression, the National Institute of Mental Health (MH082876), the National Institute on Drug Abuse (DA023988) and the National Institute of Neurological Disorders and Stroke (NS058339). We would like to thank Dr Maisie Lo and members of the Deisseroth Lab for their generosity and assistance in performing the optogenetic experiments. We thank Joe Takahashi for the *Clock* Δ 19 mice. The excellent technical assistance of Heather Buresch, Emily Webster, Edgardo Falcon, Elizabeth Gordon and Ariel Ketcherside is greatly appreciated.

AUTHOR CONTRIBUTIONS

MMS designed experiments, performed and analyzed the optogenetic, western blotting and behavioral studies, assisted with the electrophysiology experiments and wrote the paper. SS performed the PCR and ChIP assays, collected tissue for western blotting, analyzed data and contributed to writing of the paper. KD performed the electrophysiology experiments with assistance by SK and contributed to writing of the appropriate sections. PKP performed immunohistochemistry and provided feedback on the manuscript. KT and MRW provided technical assistance and conceptual advice with optogenetic experiments along with KD, and provided substantial feedback on the manuscript. RA provided technical assistance with the PCR and ChIP assays. JFE and EMR performed the luciferase assays. JPRJ and MC provided dopamine synthesis data. CAM was responsible for designing and supervising the experiments, providing conceptual guidance and for editing of the manuscript.

REFERENCES

- 1 McClung CA. Circadian genes, rhythms and the biology of mood disorders. *Pharmacol Ther* 2007; **114**: 222–232.
- 2 Plante DT, Winkelman JW. Sleep disturbance in bipolar disorder: therapeutic implications. *Am J Psychiatry* 2008; **165**: 830–843.
- 3 Roybal K, Theobald D, Graham A, DiNieri JA, Russo SJ, Krishnan V *et al*. Mania-like behavior induced by disruption of CLOCK. *Proc Natl Acad Sci USA* 2007; **104**: 6406–6411.
- 4 Gekakis N, Staknis D, Nguyen HB, Davis FC, Wilsbacher LD, King DP *et al*. Role of the CLOCK protein in the mammalian circadian mechanism. *Science* 1998; **280**: 1564–1569.

- 5 King DP, Vitaterna MH, Chang AM, Dove WF, Pinto LH, Turek FW *et al*. The mouse Clock mutation behaves as an antimorph and maps within the W(19H) deletion, distal of Kit. *Genetics* 1997; **146**: 1049–1060.
- 6 McClung CA, Sidiropoulou K, Vitaterna M, Takahashi JS, White FJ, Cooper DC *et al*. Regulation of dopaminergic transmission and cocaine reward by the Clock gene. *Proc Natl Acad Sci USA* 2005; **102**: 9377–9381.
- 7 Coque L, Mukherjee S, Cao J-L, Spencer S, Marvin M, Falcon E *et al*. Specific role of VTA dopamine neuronal firing rates and morphology in the reversal of anxiety-related, but not depression-related behavior in the Clock(Delta)19 mouse model of mania. *Neuropsychopharmacology* 2011; **36**: 1478–1488.
- 8 Cousins DA, Butts K, Young AH. The role of dopamine in bipolar disorder. *Bipolar Disord* 2009; **11**: 787–806.
- 9 Mukherjee S, Coque L, Cao J-L, Kumar J, Chakravarty S, Asaithamby A *et al*. Knockdown of Clock in the ventral tegmental area through RNA interference results in a mixed state of mania and depression-like behavior. *Biol Psychiatry* 2010; **68**: 503–511.
- 10 Tsai H-C, Zhang F, Adamantidis A, Stuber GD, Bonci A, de Lecea L *et al*. Phasic firing in dopaminergic neurons is sufficient for behavioral conditioning. *Science* 2009; **324**: 1080–1084.
- 11 Grace AA, Bunney BS. Intracellular and extracellular electrophysiology of nigral dopaminergic neurons—3. Evidence for electrotonic coupling. *Neuroscience* 1983; **10**: 333–348.
- 12 White FJ. Synaptic regulation of mesocorticolimbic dopamine neurons. *Annu Rev Neurosci* 1996; **19**: 405–436.
- 13 Dzirasa K, Ribeiro S, Costa R, Santos LM, Lin SC, Grosmark A *et al*. Dopaminergic control of sleep-wake states. *J Neurosci* 2006; **26**: 10577–10589.
- 14 Dzirasa K, Fuentes R, Kumar S, Potes JM, Nicolelis MA. Chronic in vivo multi-circuit neurophysiological recordings in mice. *J Neurosci Methods* 2011; **195**: 36–46.
- 15 Yizhar O, Fenno LE, Prigge M, Schneider F, Davidson TJ, O'Shea DJ *et al*. Neocortical excitation/inhibition balance in information processing and social dysfunction. *Nature* 2011; **477**: 171–178.
- 16 Mobley JaV-D T. Optical Properties of Tissue. *Biomedical Photonics Handbook*. CRC Press: Boca Raton, FL, 2003 pp 2–76.
- 17 Aravanis AM, Wang LP, Zhang F, Meltzer LA, Mogri MZ, Schneider MB *et al*. An optical neural interface: in vivo control of rodent motor cortex with integrated fiberoptic and optogenetic technology. *J Neural Eng* 2007; **4**: S143–S156.
- 18 Tye KM, Prakash R, Kim SY, Fenno LE, Grosenick L, Zarabi H *et al*. Amygdala circuitry mediating reversible and bidirectional control of anxiety. *Nature* 2011; **471**: 358–362.
- 19 Maywood ES, Fraenkel E, McAllister CJ, Wood N, Reddy AB, Hastings MH *et al*. Disruption of peripheral circadian timekeeping in a mouse model of Huntington's disease and its restoration by temporally scheduled feeding. *J Neurosci* 2010; **30**: 10199–10204.
- 20 Tsankova NM, Kumar A, Nestler EJ. Histone modifications at gene promoter regions in rat hippocampus after acute and chronic electroconvulsive seizures. *J Neurosci* 2004; **24**: 5603–5610.
- 21 Lena I, Parrot S, Deschaux O, Muffat-Joly S, Sauvinet V, Renaud B *et al*. Variations in extracellular levels of dopamine, noradrenaline, glutamate, and aspartate across the sleep-wake cycle in the medial prefrontal cortex and nucleus accumbens of freely moving rats. *J Neurosci Res* 2005; **81**: 891–899.
- 22 Maloney KJ, Mainville L, Jones BE. c-Fos expression in dopaminergic and GABAergic neurons of the ventral mesencephalic tegmentum after paradoxical sleep deprivation and recovery. *Eur J Neurosci* 2002; **15**: 774–778.
- 23 Naylor E, Bergmann BM, Krauski K, Zee PC, Takahashi JS, Vitaterna MH *et al*. The circadian Clock mutation alters sleep homeostasis in the mouse. *J Neurosci* 2000; **20**: 8138–8143.
- 24 Haycock JW, Haycock DA. Tyrosine hydroxylase in rat brain dopaminergic nerve terminals. Multiple-site phosphorylation in vivo and in synaptosomes. *J Biol Chem* 1991; **266**: 5650–5657.
- 25 Kumer SC, Vrana KE. Intricate regulation of tyrosine hydroxylase activity and gene expression. *J Neurochem* 1996; **67**: 443–462.
- 26 Aumann TD, Egan K, Lim J, Boon WC, Bye CR, Chua HK *et al*. Neuronal activity regulates expression of tyrosine hydroxylase in adult mouse substantia nigra pars compacta neurons. *J Neurochem* 2011; **116**: 646–658.
- 27 Webb IC, Baltazar RM, Wang X, Pitchers KK, Coolen LM, Lehman MN. Diurnal variations in natural and drug reward, mesolimbic tyrosine hydroxylase, and Clock gene expression in the male rat. *J Biol Rhythms* 2009; **24**: 465–476.
- 28 Lowrey PL, Takahashi JS. Genetics of circadian rhythms in Mammalian model organisms. *Adv Genet* 2011; **74**: 175–230.
- 29 Lewis-Tuffin LJ, Quinn PG, Chikaraishi DM. Tyrosine hydroxylase transcription depends primarily on cAMP response element activity, regardless of the type of inducing stimulus. *Mol Cell Neurosci* 2004; **25**: 536–547.
- 30 Dunkley PR, Bobrovskaya L, Graham ME, von Nagy-Felsobuki EI, Dickson PW. Tyrosine hydroxylase phosphorylation: regulation and consequences. *J Neurochem* 2004; **91**: 1025–1043.

- 31 Bobrovskaya L, Gilligan C, Bolster EK, Flaherty JJ, Dickson PW, Dunkley PR. Sustained phosphorylation of tyrosine hydroxylase at serine 40: a novel mechanism for maintenance of catecholamine synthesis. *J Neurochem* 2007; **100**: 479–489.
- 32 Kim TI, McCall JG, Jung YH, Huang X, Siuda ER, Li Y *et al*. Injectable, cellular-scale optoelectronics with applications for wireless optogenetics. *Science* 2013; **340**: 211–216.
- 33 Tye KM, Mirzabekov JJ, Warden MR, Ferenczi EA, Tsai HC, Finkelstein J *et al*. Dopamine neurons modulate neural encoding and expression of depression-related behaviour. *Nature* 2013; **493**: 537–541.
- 34 Chaudhury D, Walsh JJ, Friedman AK, Juarez B, Ku SM, Koo JW *et al*. Rapid regulation of depression-related behaviours by control of midbrain dopamine neurons. *Nature* 2013; **493**: 532–536.
- 35 Yizhar O, Fenno LE, Davidson TJ, Mogri M, Deisseroth K. Optogenetics in neural systems. *Neuron* 2011; **71**: 9–34.
- 36 Berndt A, Yizhar O, Gunaydin LA, Hegemann P, Deisseroth K. Bi-stable neural state switches. *Nat Neurosci* 2009; **12**: 229–234.
- 37 Gekakis N, Staknis D, Nguyen HB, Davis FC, Wilsbacher LD, King DP *et al*. Role of the CLOCK protein in the mammalian circadian mechanism. *Science* 1998; **280**: 1564–1569.
- 38 Shimomura K, Kumar V, Koike N, Kim TK, Chong J, Buhr ED *et al*. Usf1, a suppressor of the circadian Clock mutant, reveals the nature of the DNA-binding of the CLOCK:BMAL1 complex in mice. *Elife* 2013; **2**: e00426.
- 39 Kumar S, Chen D, Sehgal A. Dopamine acts through Cryptochrome to promote acute arousal in *Drosophila*. *Genes Dev* 2012; **26**: 1224–1234.
- 40 Chung S, Lee EJ, Yun S, Choe HK, Park SB, Son HJ *et al*. Impact of circadian nuclear receptor REV-ERBalpha on midbrain dopamine production and mood regulation. *Cell* 2014; **157**: 858–868.
- 41 Sidor MM, MacQueen GM. Antidepressants for the acute treatment of bipolar depression: a systematic review and meta-analysis. *J Clin Psychiatry* 2011; **72**: 156–167.
- 42 Sidor MM, MacQueen GM. An update on antidepressant use in bipolar depression. *Curr Psychiatry Rep* 2012; **14**: 696–704.
- 43 Geddes JR, Miklowitz DJ. Treatment of bipolar disorder. *Lancet* 2013; **381**: 1672–1682.

Supplementary Information accompanies the paper on the Molecular Psychiatry website (<http://www.nature.com/mp>)